(Received 8 February 2026, Accepted 16 March 2026, Scheduled 20 April 2026)

Wide Stopband Filtering Power Divider Based on Stepped-Impedance Open Stub and Three-Line Coupled Structures

Chuanyun Wang[1], Qian Cao[1], and Pin Wen[1, 2, *]

[1] School of Information and Software Engineering, East China Jiaotong University, Nanchang 330013, China
[2] School of Information Engineering, Nanchang University, Nanchang 330031, China

ABSTRACT: A novel wide-stopband filtering power divider (FPD) is proposed in this paper. The proposed wide stopband FPD integrates a pair of three-line coupled structures (TLCSs)-based bandpass filters (BPFs) and stepped-impedance open stubs. This topology achieves a wide stopband through harmonic suppression and enhanced filtering simultaneously. Specifically, the stepped-impedance open stubs effectively suppress harmonics to extend the stopband while also improving in-band impedance matching. Concurrently, the TLCS-based BPFs generate multiple transmission zeros (TZs) on both sides of the passband, improving frequency selectivity. A prototype wide stopband FPD operating at 3.5 GHz is fabricated and measured. There is a favorable agreement between the measured and simulated results, displaying a stopband up to 15 GHz ($4.3\,f_0$), which features a rejection level of -15.8 dB and -10 dB fractional bandwidths of 44.8%.

1. INTRODUCTION

Modern wireless communication systems have strict requirements for circuit size and communication quality, and the development of microwave passive components toward integration and miniaturization has become a research hotspot. As a crucial type of passive component, power dividers have gained widespread attention. Meanwhile, filter power dividers (FPDs), which integrate filtering functionality, are currently the focus of research [1–9]. There are two methods for designing an FPD. A power divider is cascaded with a filter in the first method [4, 5], and a power divider and a filter are integrated in the second method [6]. When the first method is adopted, directly cascading the filter and power divider will introduce additional insertion loss. In contrast, the second method, relying on an integrated design, can not only reduce insertion loss but also make the circuit size more compact. Thanks to this advantage, the second method has gradually become the mainstream research direction among contemporary scholars.

As the pursuit of high-performance and interference-free communication intensifies, the research and development activities carried out for FPDs with wide stopband characteristics are attracting increasing attention. At present, a range of methods have been developed to realize wide stopband FPDs, such as stepped-impedance parallel coupling lines instead of traditional $\lambda/4$ transmission lines [10, 11] and etching different defected ground structures (DGSs) on the ground plane utilizing slow wave effect [12, 13]. Moreover, discriminating coupling structure [14], short-circuited half-wavelength resonators [15], and mixed electric and magnetic coupling structure [16] were employed to suppress harmonic signals, thus realizing wide stopbands for FPDs. In [17], researchers adopt a pair of half-wavelength open stubs, and this design allows high frequency selectivity to be achieved. The output ports are loaded with two additional open stubs, which can generate multiple transmission zeros and enhance upper stopband rejection. In [18], to achieve the design objectives of a steep passband cut-off and high upper stopband rejection, the research team utilized a pair of short-ended coupled line stubs to realize the introduction of multiple transmission poles and zeros. However, in [17] and [18], the same drawback is also observed, namely that the stopband bandwidth performance is deficient. Three-line coupled structures (TLCSs) were first analyzed in [21]. The wideband bandpass filtering power divider (WBFPD) is designed using a wideband bandpass filter based on an asymmetric stepped impedance resonator. Parallel coupled microstrip lines are used to create both a wideband filtering characteristic and two additional transmission poles [22]. Five-coupled-lines [23] (FCLs) were first introduced for designing wideband FPD. Stepped-impedance transmission lines are adopted to replace quarter-wavelength transmission lines for bandwidth expansion [24].

This paper designs and proposes a novel wide-stopband FPD, and the components of this wide-stopband FPD include stepped-impedance open stubs and band-pass filters (BPFs) carefully designed based on the three-line coupled-line structure. This design's unique advantages lie in the fact that stepped-impedance open stubs achieve both stopband expansion and the optimization of impedance matching within the passband range. At the same time, the pair of BPFs based on TLCS can generate controllable transmission zeros. To verify the feasibility of this design idea, this paper has finally fabricated a prototype sample of the wide-stopband FPD and conducted tests.

* Corresponding author: Pin Wen (wenpin925@hotmail.com).

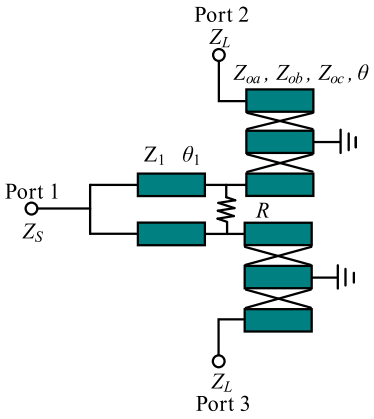

FIGURE 1. Schematic of the initial FPD.

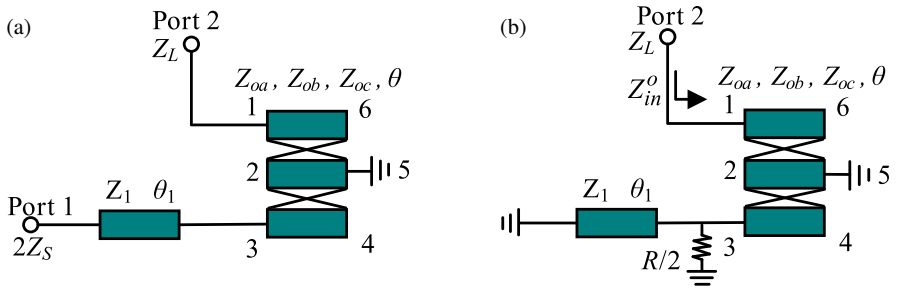

FIGURE 2. Equivalent circuit of the initial FPD. (a) Even mode circuit. (b) Odd mode circuit.

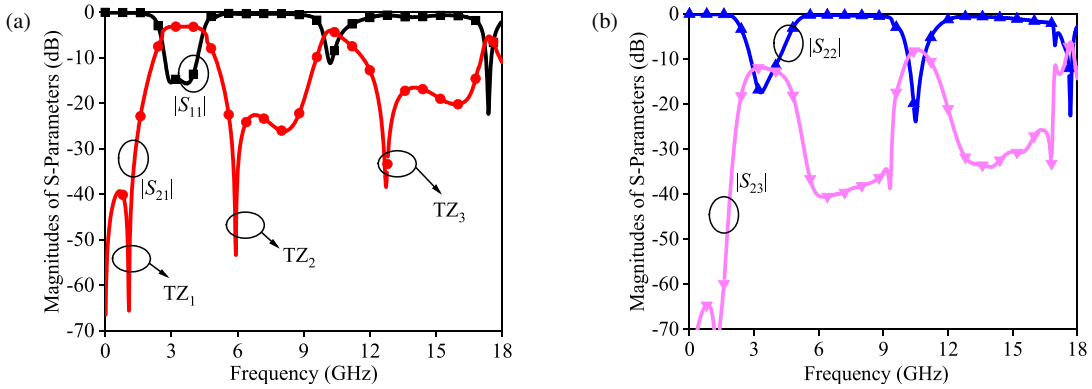

FIGURE 3. Simulation results of the initial FPD: (a) S_{11}, S_{21}. (b) S_{22}, S_{23}.

2. THE INITIAL FPD

Figure 1 illustrates the schematic of the initial FPD. This initial FPD is composed of a traditional Wilkinson power divider and a pair of TLCS-based BPFs. The pair of TLCS-based BPFs is respectively placed at port 2 and port 3. This TLCS's transmission properties can be characterized with three fundamental impedance modes, which are Z_{oa}, Z_{ob}, and Z_{oc}. Every transmission line and coupled line are equal to $\pi/2$, which is defined as the quarter wavelength ($\lambda/4$). The impedance at both output ports is defined as Z_L, and the impedance at port 1 is denoted as Z_S. Results of the even and odd-mode analysis on the initial FPD are presented in Figs. 2(a) and (b), respectively. Fig. 2(a) presents the even-mode equivalent circuit, from which the modal equations ($I_2 = I_4 = I_6 = 0$, $V_5 = 0$) can be derived. Through substituting them into the six-port scattering (S) matrix based on voltage and current [19], the impedance (Z) parameters of the two-port even-mode equivalent circuit, i.e., Z^e_{11}, Z^e_{12}, Z^e_{21}, and Z^e_{22}, can be derived. For $i, j \in \{1, 3, 5\}$, the impedance parameter Z_{ij} is defined as the ratio of the voltage at port i to the current injected into port j, with all other ports open-circuited

$$Z^e_{11} = Z_{11} - \frac{Z_{15}Z_{51}}{Z_{55}} \tag{1}$$

$$Z^e_{12} = Z_{13} - \frac{Z_{15}Z_{53}}{Z_{55}} \tag{2}$$

$$Z^e_{21} = Z_{31} - \frac{Z_{35}Z_{51}}{Z_{55}} \tag{3}$$

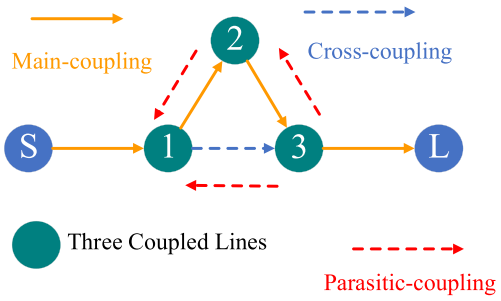

FIGURE 4. Coupling topology of the initial FPD.

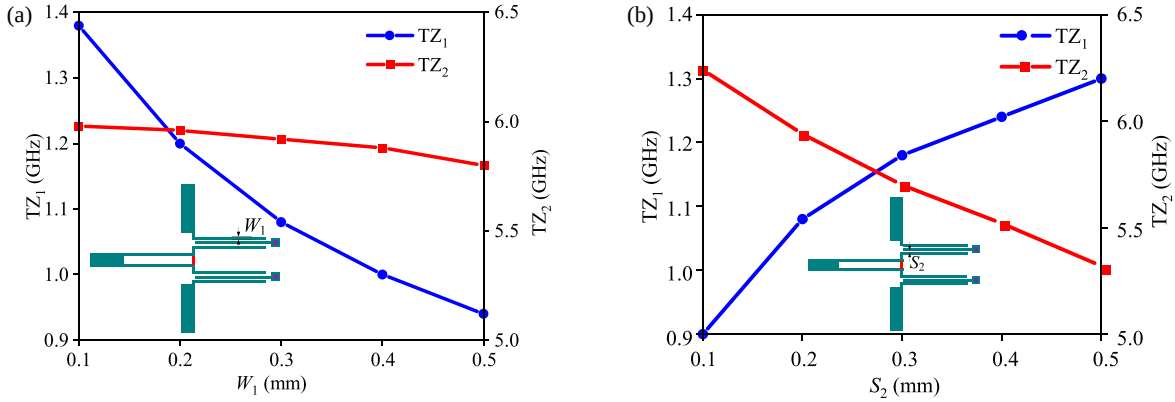

FIGURE 5. Variations of TZ_1 and TZ_2 with different parameters: (a) Variation with W_1. (b) Variation with S_2.

$$Z_{22}^e = Z_{33} - \frac{Z_{35}Z_{53}}{Z_{55}} \tag{4}$$

This enables the derivation of the following: under the condition of even-mode excitation, the reflection coefficients ($|S_{11}^e|$ and $|S_{22}^e|$) at port 1 and port 2 as well as the transmission coefficient $|S_{22}^e|$ of the initial FPD. Additionally, by referring to the modal equations ($I_2 = I_4 = I_6 = 0$, $V_5 = 0$, $V_3 = -I_4 Z_1 R/(2Z_1 + R)$) of the odd-mode equivalent circuit in Fig. 2(b), the odd-mode input-impedance Z_{in}^o can be obtained.

$$Z_{in}^o = Z_o^c \frac{Z_L + jZ_{oc}\tan\theta}{Z_{oc} + jZ_L\tan\theta} \tag{5}$$

As a result, the reflection coefficient $|S_{22}^o|$ of port 2 under odd-mode excitation is

$$|S_{22}^o| = \frac{Z_{in}^o - Z_L}{Z_{in}^o + Z_L} \tag{6}$$

Accordingly, the frequency responses of the initial FPD can be obtained as [20]

$$\begin{aligned} |S_{11}| &= |S_{11}^e| \\ &= \frac{(Z_{11}^e - 2Z_S - Z_1)(Z_{22}^e + Z_L) - Z_{12}^e Z_{21}^e}{(Z_{11}^e + 2Z_S + Z_1)(Z_{22}^e + Z_L) - Z_{21}^e Z_{12}^e} \end{aligned} \tag{7}$$

$$\begin{aligned} |S_{21}| &= |S_{21}^e|/\sqrt{2} \\ &= \frac{2Z_{21}^e\sqrt{Z_L\left(\frac{Z_1}{2} + Z_S\right)}}{(Z_{11}^e + 2Z_S + Z_1)(Z_{22}^e + Z_L) - Z_{21}^e Z_{12}^e} \end{aligned} \tag{8}$$

$$|S_{22}| = \frac{S_{22}^e + S_{22}^o}{2} \tag{9}$$

$$|S_{23}| = \frac{S_{22}^e - S_{22}^o}{2} \tag{10}$$

To facilitate the clear observation of the frequency response characteristics of the initial FPD, corresponding simulation results are presented in Fig. 3.

As observed from Fig. 3(a), TZ_1 (1.08 GHz) and TZ_2 (5.94 GHz) are on both sides of the passband, and TZ_3 (12.42 GHz) is situated in the stopband. The transmission zeros on both sides of the passband provide excellent frequency selectivity. As depicted in Fig. 3(b), the proposed structure realizes excellent in-band isolation across the operating band and favorable matching performance at the output port.

TZ_3 is a parasitic zero caused by parasitic coupling. Cross-coupling within the compact TLCS gives rise to the transmission zeros located on both sides of the passband. Fig. 4 illustrates the topology of the three-line coupled line, in which the cross coupling and parasitic coupling are clearly shown. In the adopted three-line coupling structure, 1 denotes the bottom coupling line, 2 denotes the middle short-circuited coupling line, and 3 denotes the top coupling line.

Figure 5(a) indicates that the low-frequency transmission zero TZ_1 decreases as the length of W_1 increases, with no significant change observed in the high-frequency transmission zero TZ_2. In Fig. 5(b), the low-frequency transmission zero TZ_1 increases with the increasing length of S_2, and the high-frequency transmission zero TZ_2 decreases as the length of S_2 grows.

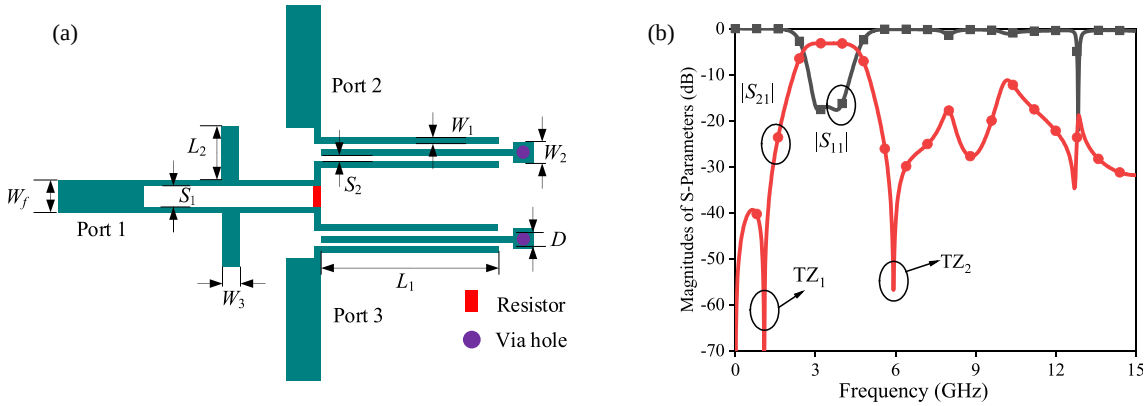

FIGURE 6. (a) Integrate uniform stepped-impedance open stubs. (b) Simulation results: S_{11}, S_{21}.

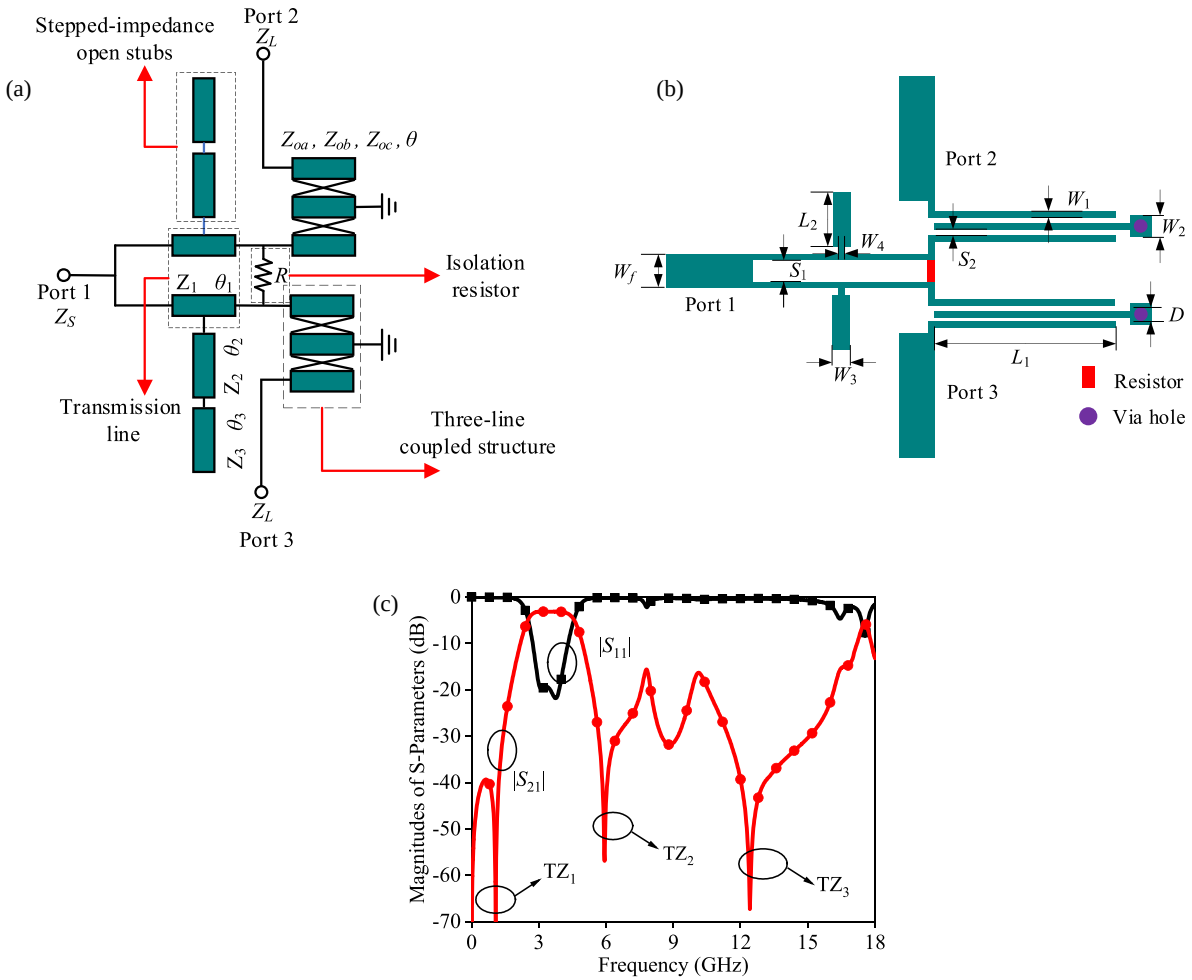

FIGURE 7. (a) Schematic of the wide stopband FPD. (b) Layout of the wide stopband FPD. (c) Simulation results: S_{11}, S_{21}.

3. THE PROPOSED WIDE STOPBAND FPD

The initial FPD is designed in Section 2. To address the issues of harmonic interference and improve impedance matching within the passband, as shown in Fig. 6(a), first, uniform-impedance open stubs are integrated at the central position of the $\lambda/4$ transmission lines. The simulation results are shown in Fig. 6(b). It can be observed that the out-of-band suppression is poor. Subsequently, a wide stopband FPD is proposed by integrating stepped-impedance open stubs (Z_2, θ_2 and Z_3, θ_3) at the central position of the $\lambda/4$ transmission lines. The combination of this $\lambda/4$ transmission line and the loaded stepped-impedance open stub forms a low-pass filter structure. This low-pass filter can effectively suppress the harmonic frequencies in the stopband and improve the impedance matching within the passband.

The schematic and layout of the wide-stopband FPD are presented in Figs. 7(a) and (b), respectively. The simulation results of the wide stopband FPD are shown in Fig. 7(c). As illustrated in Fig. 7(c), the TZ$_1$ and TZ$_2$ are unchanged, which

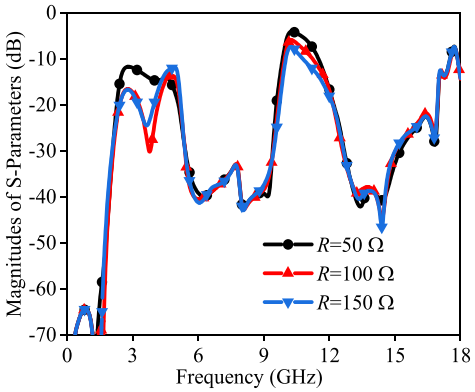

FIGURE 8. Effect of loading resistance on isolation.

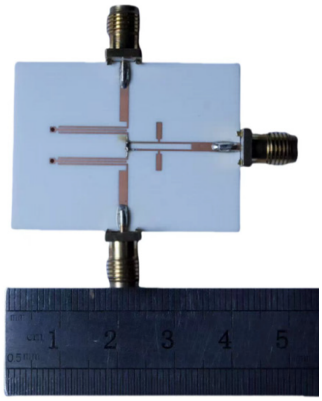

FIGURE 9. Prototype of the proposed wide stopband FPD.

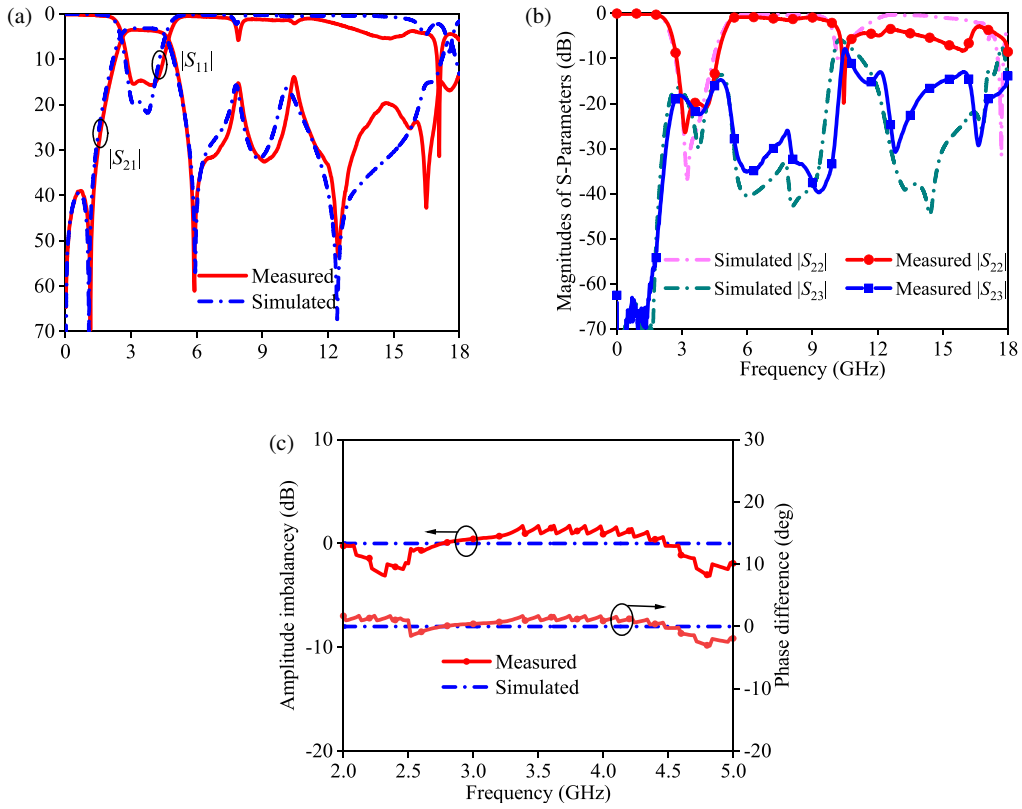

FIGURE 10. The simulated and measured results of the wide stopband FPD. (a) Results of S_{11}, S_{21}. (b) Results of S_{22} and S_{23}. (c) Results of phase difference and amplitude imbalance.

presents high frequency selectivity, and the attenuation level of TZ_3 is significantly increased to 67 dB, showing a stopband up to $4.3f_0$ with 15.8 dB rejection level. Fig. 8 illustrates the variation of isolation with different values of the isolation resistor. With the isolation resistor rising in value from 50 Ω to 150 Ω, the isolation performance first improves and then deteriorates. Therefore, the resistor is set at 100 Ω, resulting in markedly enhanced signal isolation between output ports.

4. RESULTS AND DISCUSSION

To verify the aforementioned analytical results, this wide stopband FPD is fabricated on a Rogers RO4003 substrate with a thickness of 0.813 mm, relative permittivity of 3.55, and loss tangent of 0.0027. The photograph of the proposed wide stopband FPD is depicted in Fig. 9. All key physical parameters of the wide stopband FPD designed in this work are detailed in Table 1. As presented in Fig. 10(a), the center frequency corresponding to the operating band is 3.5 GHz, and the −10 dB frac-

TABLE 1. The physical parameters of the wide stopband FPD (unit: mm).

W_f	W_1	W_2	W_3	W_4
1.58	0.3	1	1	0.3
L_1	L_2	S_1	S_2	D
12	3	0.98	0.2	0.6

TABLE 2. Comparison with previous wide stopband FPDs.

Ref.	f_0 (GHz)	FBW (%)	RL (dB)	TZs	Stopband	Circuit Size ($\lambda_g \times \lambda_g$)
[10]	2.0	49.5	> 15	4	$4.4f_0$	0.23×0.23
[16]	0.9	6.5	> 16.5	3	$2.1f_0$	0.15×0.14
[17]	3.0	65	> 29	6	$1.1f_0$	0.33×0.72
[18]	1.5	56.5	> 10.5	4	$1.42f_0$	0.32×0.32
[22]	4.0	53	> 18.5	3	$2.8f_0$	0.53×0.37
[23]	1.8	73	> 13	2	$2.5f_0$	0.39×0.11
This work	3.5	44.8	> 14.8	3	$4.3f_0$	0.56×0.75

tional bandwidth achieves a value of 44.8%. Moreover, within the operating frequency band, the insertion loss is 3.7 dB, while the return loss is greater than 14.9 dB. In Fig. 10(b), the measured isolation within the passband is greater than 17.7 dB.

From Fig. 10(c), the measured results of the amplitude imbalance and phase difference between port 2 and port 3 can be obtained. Within the passband, the value of the former is less than 0.8 dB, while that of the latter is below 2.3°. For the designed wide-stopband FPD, the results from practical measurements are basically in agreement with the simulation results. In Table 2, the parameters of the proposed wide stopband FPD are compared against the corresponding ones from other literature. All structures in Table 2 adopt the second method. Compared with [10], the fractional bandwidth and stopband performance are comparable, while the proposed structure in this work is simpler and easier to fabricate. Compared with [16], the fractional bandwidth and stopband performance of this work are superior. Compared with [17] and [22], this work has a better stopband performance. Compared with [18] and [23], this work exhibits superior return loss and stopband performance.

5. CONCLUSION

A wide-stopband FPD with high frequency selectivity is proposed. Due to the existence of cross-coupling in the TLCS, TZ_1 and TZ_2 are generated, thereby enabling the device to exhibit high frequency selectivity. The combination of these λ/4 transmission lines and the loaded stepped-impedance open stub forms a low-pass filter structure, which can expand the stopband. Meanwhile, the performance of impedance matching within the passband has also been improved to a certain extent. Finally, by connecting an isolation resistor between the two ends of the $\lambda/4$ transmission line, the isolation of the proposed wide stopband FPD can be effectively improved. The actual measurement data show that the designed wide stopband FPD has a fractional bandwidth of 44.8%, with its stopband extending up to 15 GHz (corresponding to 4.3 times the center frequency f_0 and a stopband rejection level of -15.8 dB.

In subsequent work, to expand the stopband, the following measures can be adopted: First, use multi-mode resonant structures to create transmission zeros in the stopband, which can effectively suppress harmonic signals. Second, add harmonic suppression components, such as open stubs or DGS to eliminate spurious responses.

ACKNOWLEDGEMENT

This work is funded by the Key R&D Program of Jiangxi Province, China (Nos. 20261BCE310039, 20243BBG71030).

REFERENCES

[1] Xu, K. D., Y. Bai, X. Ren, and Q. Xue, "Broadband filtering power dividers using simple three-line coupled structures," *IEEE Transactions on Components, Packaging and Manufacturing Technology*, Vol. 9, No. 6, 1103–1110, Jun. 2019.

[2] Liu, Y., L. Zhu, and S. Sun, "Proposal and design of a power divider with wideband power division and port-to-port isolation: A new topology," *IEEE Transactions on Microwave Theory and Techniques*, Vol. 68, No. 4, 1431–1438, Apr. 2020.

[3] Liu, Y., S. Sun, and L. Zhu, "2N-way wideband filtering power dividers with good isolation enhanced by a modified isolation network," *IEEE Transactions on Microwave Theory and Techniques*, Vol. 70, No. 6, 3177–3187, Jun. 2022.

[4] Wang, D., X. Guo, and W. Wu, "Wideband unequal power divider with enhanced power dividing ratio, fully matching bandwidth, and filtering performance," *IEEE Transactions on Microwave Theory and Techniques*, Vol. 70, No. 6, 3200–3212, Jun. 2022.

[5] Feng, W., Y. Zhao, W. Che, R. Gómez-García, and Q. Xue, "Single-ended-to-balanced filtering power dividers with wideband common-mode suppression," *IEEE Transactions on Microwave Theory and Techniques*, Vol. 66, No. 12, 5531–5542, Dec. 2018.

[6] Xia, Z., J. Wang, Q.-Y. Lu, W. Wu, and J. Hong, "A wideband 90° phase shifting element applied in quadrature phase filtering power divider," *IEEE Microwave and Wireless Technology Letters*, Vol. 34, No. 2, 167–170, Feb. 2024.

[7] Xu, X., D. Zheng, and F. Huang, "A new filtering out-of-phase power divider with unequal power distribution using modified branch-line structure," *IEEE Microwave and Wireless Technology Letters*, Vol. 35, No. 5, 537–540, May 2025.

[8] Guo, X., Y. Liu, and W. Wu, "Wideband unequal filtering power divider with arbitrary constant power ratio and phase difference," *IEEE Transactions on Circuits and Systems II: Express Briefs*, Vol. 70, No. 2, 421–425, Feb. 2023.

[9] Liu, H., Y. Ma, S. Zhang, S. Fang, and Z. Wang, "Wideband three-way power divider with bandpass filtering response using unequal-width three-coupled line," *AEU — International Journal of Electronics and Communications*, Vol. 151, 154229, 2022.

[10] Chen, M.-T. and C.-W. Tang, "Design of the filtering power divider with a wide passband and stopband," *IEEE Microwave and Wireless Components Letters*, Vol. 28, No. 7, 570–572, Jul. 2018.

[11] Tang, C.-W. and J.-T. Chen, "A design of 3-dB wideband microstrip power divider with an ultra-wide isolated frequency band," *IEEE Transactions on Microwave Theory and Techniques*, Vol. 64, No. 6, 1806–1811, Jun. 2016.

[12] Rao, Y., H. J. Qian, B. Yang, R. Gómez-García, and X. Luo, "Dual-band bandpass filter and filtering power divider with ultra-wide upper stopband using hybrid microstrip/DGS dual-resonance cells," *IEEE Access*, Vol. 8, 23 624–23 637, 2020.

[13] Fan, L., H. J. Qian, B. Yangl, G. Wang, and X. Luo, "Filtering power divider with wide stopband using open-stub loaded coupled-line and hybrid microstrip T-stub/DGS cell," in *2018 IEEE/MTT-S International Microwave Symposium — IMS*, 1–4, Philadelphia, PA, USA, Jun. 2018.

[14] Zhao, X.-L., L. Gao, X. Y. Zhang, and J.-X. Xu, "Novel filtering power divider with wide stopband using discriminating coupling," *IEEE Microwave and Wireless Components Letters*, Vol. 26, No. 8, 580–582, Aug. 2016.

[15] Chau, W.-M., K.-W. Hsu, and W.-H. Tu, "Wide-stopband Wilkinson power divider with bandpass response," *Electronics Letters*, Vol. 50, No. 1, 39–40, Jan. 2014.

[16] Zhang, X. Y., K.-X. Wang, and B.-J. Hu, "Compact filtering power divider with enhanced second-harmonic suppression," *IEEE Microwave and Wireless Components Letters*, Vol. 23, No. 9, 483–485, Sep. 2013.

[17] Yu, X. and S. Sun, "A novel wideband filtering power divider with embedding three-line coupled structures," *IEEE Access*, Vol. 6, 41 280–41 290, 2018.

[18] Zhu, H., A. M. Abbosh, and L. Guo, "Wideband four-way filtering power divider with sharp selectivity and wide stopband using looped coupled-line structures," *IEEE Microwave and Wireless Components Letters*, Vol. 26, No. 6, 413–415, Jun. 2016.

[19] Chen, C.-P., J. Oda, K. Kamata, W. Imashiro, T. Anada, and S. Takeda, "An iterative synthesis scheme for wideband filter based on parallel-coupled three-line," in *2013 European Microwave Conference*, 889–892, Nuremberg, Germany, Oct. 2013.

[20] Ahn, H.-R., *Asymmetric Passive Components in Microwave Integrated Circuits*, Ch. 2, John Wiley & Sons, Hoboken, NJ, USA, 2006.

[21] Yamamoto, S., T. Azakami, and K. Itakura, "Coupled strip transmission line with three center conductors," *IEEE Transactions on Microwave Theory and Techniques*, Vol. 14, No. 10, 446–461, Oct. 1966.

[22] Gorur, A. K., E. Dogan, C. Karpuz, and A. Gorur, "Wideband filtering power dividers with/without notch band," *Microwave and Optical Technology Letters*, Vol. 66, No. 3, e34091, 2024.

[23] Zhang, Y., H. Liu, S. Chen, Z. Wang, and S. Fang, "All-port-reflectionless wideband filtering power divider using five-line coupled structure," *IEEE Microwave and Wireless Technology Letters*, Vol. 35, No. 1, 31–34, 2025.

[24] Wang, C.-Y., Q. Cao, and P. Wen, "Wideband filtering power divider based on stepped-impedance transmission lines and three-line coupled structures," in *2025 Cross Strait Radio Science and Wireless Technology Conference (CSRSWTC)*, 1–3, Guangzhou, China, 2025.